

## Article

# Oxysterol 7- $\alpha$ Hydroxylase (CYP7B1) Attenuates Metabolic-Associated Fatty Liver Disease in Mice at Thermoneutrality

Ioannis Evangelakos <sup>1</sup>, Dorothee Schwinge <sup>2</sup>, Anna Worthmann <sup>1</sup>, Clara John <sup>1</sup>, Niklas Roeder <sup>1</sup>, Paul Pertzborn <sup>1</sup>, Janina Behrens <sup>1</sup>, Christoph Schramm <sup>2</sup>, Ludger Scheja <sup>1</sup> and Joerg Heeren <sup>1,\*</sup>

<sup>1</sup> Department of Biochemistry and Molecular Cell Biology, University Medical Center Hamburg-Eppendorf, 20246 Hamburg, Germany; i.evangelakos@uke.de (I.E.); a.worthmann@uke.de (A.W.); clara\_john@gmx.de (C.J.); nproeder@googlemail.com (N.R.); paulpertzborn@gmx.de (P.P.); janina.behrens.jb@googlemail.com (J.B.); l.scheja@uke.de (L.S.)

<sup>2</sup> Department of Medicine, University Medical Center Hamburg-Eppendorf, 20246 Hamburg, Germany; d.schwinge@uke.de (D.S.); c.schramm@uke.de (C.S.)

\* Correspondence: heeren@uke.de; Tel.: +49-40741051715

**Abstract:** Ambient temperature is an important determinant of both the alternative bile acid synthesis pathway controlled by oxysterol 7- $\alpha$  hydroxylase (CYP7B1) and the progression of metabolic-associated fatty liver disease (MAFLD). Here, we investigated whether CYP7B1 is involved in the etiology of MAFLD under conditions of low and high energy expenditure. For this, *Cyp7b1*<sup>-/-</sup> and wild type (WT) mice were fed a choline-deficient high-fat diet and housed either at 30 °C (thermoneutrality) or at 22 °C (mild cold). To study disease phenotype and underlying mechanisms, plasma and organ samples were analyzed to determine metabolic parameters, immune cell infiltration by immunohistology and flow cytometry, lipid species including hydroxycholesterols, bile acids and structural lipids. In WT and *Cyp7b1*<sup>-/-</sup> mice, thermoneutral housing promoted MAFLD, an effect that was more pronounced in CYP7B1-deficient mice. In these mice, we found higher plasma alanine aminotransferase activity, hyperlipidemia, hepatic accumulation of potentially harmful lipid species, aggravated liver fibrosis, increased inflammation and immune cell infiltration. Bile acids and hydroxycholesterols did not correlate with aggravated MAFLD in *Cyp7b1*<sup>-/-</sup> mice housed at thermoneutrality. Notably, an up-regulation of lipoprotein receptors was detected at 22 °C but not at 30 °C in livers of *Cyp7b1*<sup>-/-</sup> mice, suggesting that accelerated metabolism of lipoproteins carrying lipotoxic molecules counteracts MAFLD progression.

**Keywords:** bile acids; hydroxycholesterol; oxysterol; *Cyp7b1*; non-alcoholic fatty liver disease; T cells; inflammation; fibrosis; steatohepatitis; metabolic-associated fatty liver disease



**Citation:** Evangelakos, I.; Schwinge, D.; Worthmann, A.; John, C.; Roeder, N.; Pertzborn, P.; Behrens, J.; Schramm, C.; Scheja, L.; Heeren, J. Oxysterol 7- $\alpha$  Hydroxylase (CYP7B1) Attenuates Metabolic-Associated Fatty Liver Disease in Mice at Thermoneutrality. *Cells* **2021**, *10*, 2656. <https://doi.org/10.3390/cells10102656>

Academic Editor: Heather Francis

Received: 14 July 2021

Accepted: 3 October 2021

Published: 5 October 2021

**Publisher's Note:** MDPI stays neutral with regard to jurisdictional claims in published maps and institutional affiliations.



**Copyright:** © 2021 by the authors. Licensee MDPI, Basel, Switzerland. This article is an open access article distributed under the terms and conditions of the Creative Commons Attribution (CC BY) license (<https://creativecommons.org/licenses/by/4.0/>).

## 1. Introduction

Metabolic-associated fatty liver disease (MAFLD) [1] is a disease with a high burden and steadily increasing prevalence in the Western world (~25% of global population) [2], which is closely associated with obesity, insulin resistance, dyslipidemia and type 2 diabetes [3]. Starting from simple hepatic steatosis, the disease can progress to severe steatohepatitis (known also as non-alcoholic steatohepatitis (NASH)) that is characterized by additional hepatic injury, inflammation and fibrosis [4]. Despite major advances in understanding the pathogenesis of MAFLD, the molecular mechanisms that drive the transition towards chronic inflammation and fibrosis are still incompletely understood. When it comes to prevention strategies against MAFLD and associated diseases, a great emphasis is given on the reduction of circulating as well as hepatic lipids including cholesterol [5]. Cholesterol accumulation or dysregulation of its metabolism has been correlated with MAFLD in humans as well as in murine models of the disease [6]. Next to the classical

bile acid synthesis pathway that is controlled by a negative feedback regulating the key enzyme cholesterol 7- $\alpha$  hydroxylase (CYP7A1), cholesterol can also be converted to bile acids via specific hydroxycholesterol intermediates in the alternative pathway [7]. These cholesterol derivatives are 25-hydroxycholesterol (25-HC) (generated in peripheral organs by the enzyme cholesterol 25-hydroxylase) and 27-HC (primarily generated in the liver by mitochondrial sterol 27-hydroxylase (CYP27A1)). The subsequent 7- $\alpha$  hydroxylation of 25-HC and 27-HC by oxysterol 7- $\alpha$  hydroxylase (CYP7B1) is then the defining step of the alternative bile acid synthesis pathway [7]. Recently, we demonstrated that housing mice at a low environmental temperature is characterized by higher flux of cholesterol to the liver [8,9], where the induction of CYP7B1 facilitates the conversion to bile acids [10]. This previously unappreciated homeostatic mechanism protects from peripheral and hepatic cholesterol accumulation and could be beneficial against fatty liver and MAFLD [11].

Oxysterols and bile acids have been described to modulate immune cell plasticity and differentiation. For instance, 25-HC has been shown to inhibit the type 1 interferon response via a negative feedback [12], while 27-HC stimulates pro-inflammatory processes via interaction with the estrogen receptor [13]. Moreover, the binding of oxidized cholesterol derivatives to the retinoic acid receptor-related orphan receptor  $\gamma$  (ROR $\gamma$ t) stimulates the differentiation of TH17 cells [14]. Further modification to sulfated sterol derivatives resulted in enhanced ROR $\gamma$ t binding while Th17 inhibitory sterol receptor liver X receptor (LXR) activity was reduced by these metabolites [15,16]. Recent papers indicate that specific bile acid species also modulate immune cell function. For example, the secondary bile acid 3-oxo lithocholic acid (LCA) suppressed the differentiation of regulatory Th17 cells, while isoallo-LCA promoted the differentiation of regulatory T cells via activation of the master transcriptional regulator Foxp3 [17]. Moreover, it was reported that diet-dependent induction of a distinct population of Foxp3-positive Treg cells is regulated by secondary bile acids via activation of the vitamin D receptor [18]. Next to nuclear receptors, G protein-coupled bile acid receptors (such as TGR5) regulate immune cells in various organs. For instance, the TGR5 ligand LCA reduces pro-inflammatory signaling pathways in macrophages of the liver [19]. Notably, CYP7B1 influences concentrations of hydroxycholesterol and bile acid species, suggesting that the enzyme could affect immune cell abundance and plasticity in chronic inflammatory metabolic disorders such as NASH.

In this context, it has been increasingly recognized that conventional housing temperature (22 °C) exposes mice to a mild cold stress that requires substantial energy expenditure to maintain body core temperature, favors metabolic homeostasis and protects against the development of metabolic disorders [20,21]. In contrast, an ambient temperature of approximately 30 °C is thermoneutral for mice, meaning that no extra energy is required for heat production. This condition has recently been recognized to promote metabolic disease development in mice, which allows better translation of experimental observations to humans who usually prefer to stay warm [20,22]. Supporting the above, it was recently shown that mild cold stress (22 °C) halts the progression of MAFLD whereas thermoneutrality (30 °C) exacerbates its development and leads to a more human-like liver phenotype [23]. These studies highlight the relevance of housing temperatures when studying metabolic disease in mice, as high energy expenditure observed at regular housing temperature could mask disease mechanisms that are present in humans.

The aim of this study was to investigate how substrates and metabolites of CYP7B1 can affect diet-induced MAFLD under conventional as well as thermoneutral conditions. Here, we show that steatohepatitis and fibrosis was more pronounced at 30 °C. At conventional room temperature, Cyp7b1<sup>-/-</sup> and wild type littermate controls have a similar phenotype. In contrast, at thermoneutrality MAFLD progression is more severe in Cyp7b1<sup>-/-</sup> mice than in controls. This phenotype correlates with markers of insulin resistance, distinct changes in the hydroxycholesterol pattern and liver infiltration of pro-inflammatory immune cells. Overall, these results indicate that CYP7B1 protects against diet-induced MAFLD progression in mice housed at thermoneutrality.

## 2. Materials and Methods

### 2.1. Experimental Animals, Housing Conditions, Diets and Animal Experiments

All mouse experiments were approved by the Animal Welfare Officers of University Medical Centre Hamburg-Eppendorf (UKE) and Behörde für Gesundheit und Verbraucherschutz Hamburg (G96/15). *Cyp7b1*<sup>-/-</sup> mice were bred and housed in the animal facility of the UKE at 22 °C under a day-night cycle of 12 h and ad libitum access to drinking water and regular chow diet (P1324, Altromin, Germany). For our study, male age-matched *Cyp7b1*<sup>-/-</sup> and WT littermates (11–12 weeks-old in the beginning of the experiment) were fed for a period of 8 months with a choline deficient high fat diet (CD-HFD, Research Diets; D05010402). At the end of the study, EDTA blood was harvested after a 4 h fasting period. Subsequently, animals were perfused with PBS and tissues were either conserved in TriFast reagent (Peqlab, Erlangen, Germany) for RNA analysis, fixed in 3.7% formaldehyde solution for histology or snap frozen and stored at −80 °C for lipid and protein analysis. Body composition analysis was performed 1 week before the end of the experiment by echoMRI.

### 2.2. Plasma Parameters

Plasma was isolated by centrifugation of EDTA-spiked blood for 10 min at 10,000 rpm at 4 °C in a bench top centrifuge. Plasma cholesterol and triglycerides were determined using commercial colorimetric kits (Roche, Mannheim, Germany) that were adapted to 96-well microtiter plates with Precipath (Roche, Mannheim, Germany) as standard. Free fatty acids (FFAs) were determined using the NEFA-HR(2) Assay (FUJIFILM). For lipoprotein profiling, 200 µL plasma was separated by fast-performance liquid chromatography (FPLC) on a Superose 6 10/300 GL column (GE Healthcare, München, Germany) with a flow rate of 0.5 mL/min. Fractions were collected and triglyceride and cholesterol concentrations were measured as described above. Plasma insulin levels were measured with an ELISA kit (#90060, ChrystalChem, Zaandam, The Netherlands) according to the manufacturers protocol. For assessment of liver damage, plasma activity of alanine aminotransferase (ALT) was determined using a photometric ALT Activity Assay (MAK052, Sigma-Aldrich, Darmstadt, Germany). Plasma albumin levels were quantified photometrically with reagents provided by Siemens Healthcare [24].

### 2.3. Bile Acid Measurement

Bile acids were quantified by HPLC coupled to electrospray ionization tandem mass spectrometry [25]. Briefly, portal plasma samples were prepared by a simple methanol liquid-liquid extraction. Quantitative measurement of bile acids was performed using a LC-ESI-QqQ system run multiple reaction monitoring (MRM) mode. HPLC analysis was performed using NEXERA X2 LC-30AD HPLC PUMP (Shimadzu, Tokyo, Japan) equipped with a Kinetex C18 column (100 Å, 150 mm × 2.1 mm i.d., Phenomenex, Torrance, CA, USA). For HPLC a mobile phase A consisting of water and a mobile phase B consisting of acetonitrile methanol (3/1 v/v) both enriched with 0.1% formic acid and 20 mM ammonium acetate was used. The column was coupled to QqQ: Q trap 5500 System (SCIEX, Darmstadt, Germany). Peaks were identified and quantified by comparing retention times, as well as MRM transitions and peak areas, respectively, to particular corresponding standard chromatograms.

### 2.4. Liver Lipid and Hydroxycholesterol Analysis

Lipid analysis of structural and storage lipids was performed using the Lipidizer platform from SCIEX (Framingham, MA, USA). Briefly, snap-frozen liver samples were homogenized and extracted using MTBE/methanol. Lipidizer Internal Standards were added to all samples during lipid extraction. Lipid extracts were concentrated and reconstituted in running buffer containing 10 mM ammonium acetate, dichloromethane/methanol (50/50). Lipid species were separated by SELEX ion technology and quantified using an ESI-QqQ system operated in multiple reaction monitoring (MRM) mode (QTRAP 5500; SCIEX) employing the Lipidizer software. Hepatic hydroxycholesterols were analyzed

after derivatization with Girard *p* reagent as previously described [26]. Targeted analysis via HPLC coupled to electrospray ionization tandem mass spectrometry was subsequently performed. Briefly, liver samples (approx. 100–150 mg) were homogenized in chloroform/methanol (1:1, *v/v*) and the resulting extracts were vacuum-dried. After resuspension in ethanol, samples were fractionated using reversed phase solid phase extraction (SPE) to enrich oxysterols devoid of cholesterol (Sep-Pak cartridges, Waters, Milford, MA, USA). Subsequently, oxysterols were derivatized with Girard P reagent followed by another SPE clean-up to deplete excess Girard P reagent. Oxysterols were separated on a hypersil GOLD reversed phase column (50 × 2.1 mm, 1.9 μm; Thermo Fisher Scientific, Waltham, MA, USA) using 49.9% H<sub>2</sub>O, 33.3% methanol, 16.7% acetonitrile and 0.1% formic acid as mobile phase A and 4.9% H<sub>2</sub>O, 63.3% methanol, 31.7% acetonitrile and formic acid 0.1% as mobile phase B. The HPLC (NEXERA X2 LC-30AD HPLC PUMP; Shimadzu, Tokyo, Japan) was coupled to a QqQ: Q trap 5500 System (SCIEX, Darmstadt, Germany), run in MRM mode. Quantification was achieved by comparing retention times, MRM transitions and peak areas to corresponding standard chromatograms.

### 2.5. Gene Expression Analysis

Total RNA was isolated using a NucleoSpin RNA II kit (Macherey & Nagel, Düren Germany). After synthesis of cDNA with SuperScript III Reverse Transcriptase (Invitrogen, Waltham, MA, USA), quantitative real-time PCR was performed and the relative expression of genes of interest was calculated by normalization to housekeeper TATA-box binding protein (Tbp). The following TaqMan Assay-on-Demand primer sets (Applied Biosystems, Waltham, MA, USA) were used: Tbp: Mm00446973\_m1; Cyp7a1: Mm00484150\_m1; Cyp7b1: Mm00484157\_m1; Cyp27a1: Mm00470430\_m1; Cyp8b1: Mm00501637\_s1; Baat: Mm00476075\_m1; Abcb11: Mm00445168\_m1; Nr0b2 (Shp): Mm00442278\_m1; Ch25h: Mm00515486\_s1; Il1b: Mm00434228\_m1; Il6: Mm00446190\_m1; Cxcl1: Mm00433859\_m1; Cxcl9: Mm00434946\_m1; Cxcl10: Mm00445235\_m1; Tnf: Mm00443258\_m1; Ccl2: Mm00441242\_m1; Ccl5: Mm01302428\_m1; Cd68: Mm03047343\_m1; Acta2: Mm00725412\_s1; Tgfb1: Mm00441724\_m1; Col1a1: Mm00801666\_g1; Timp1: Mm00441818\_m1; Mmp13: Mm00439491\_m1; Mmp12: Mm00500554\_m1; Fasn: Mm00662319\_m1; Scd1: Mm00772290\_m1; Acaca: Mm01304285\_m1; Pparg: Mm00440945\_m1; Abcg5: Mm00446249\_m1; Abcg8: Mm00445970\_m1; Ldlr: Mm00440169\_m1; Lrp1: Mm00464608\_m1; Sult2a1: Mm04205657\_mH; Sult2b1: Mm00450550\_m1; Trem2: Mm00451744\_m1. Cd9 and Gpnmb expression were assessed using SYBR green primers which were premixed with SYBR Green PCR Master Mix (Applied Biosystems). The following primer pairs were used: Cd9 forward primer: 5'-TGCTGGGATTGTTCTTCGGG-3', Cd9 reverse primer: 5'-GCTTTGAGTGTTCCCGCTG-3', Gpnmb forward primer: 5'-GAGCACAACCAATTACGTGGCT-3', Gpnmb reverse primer: 5'-GGTGATATTGGAACCCACCAGA-3', Tbp forward primer: 5'-CTTCCTGCCACAATGTCACAG-3', Tbp reverse primer: 5'-CCTTCTCATGCTTGCTTCTCTG-3'.

### 2.6. Western Blot Analysis

For SDS-PAGE samples were homogenized in a tissue lyser (Qiagen) by adding a 10× fold excess of (*v/v*) RIPA buffer (50 mM Tris-HCl pH 7.4, 5 mM EDTA, 150 mM sodium chloride, 1 mM sodium pyrophosphate, 1 mM sodium fluoride, 1 mM sodium orthovanadate, 1% NP-40) supplemented with cOmplete™ Mini Protease Inhibitor Cocktail (Roche) and Phosphatase Inhibitor Cocktail (Bimake.com). Lysates were centrifuged at 16,000 × *g* for 10 min, the clear soluble middle layer without the fat was taken, and protein concentration was determined using an adapted Lowry method [8]. 20 μg of total protein in NuPAGE reducing sample buffer (Invitrogen) were denatured at 60 °C for 10 min and separated on 10% SDS-polyacrylamide Tris-glycine gels. Transfer to nitrocellulose membranes was performed in a wet blotting system, membranes were stained with Ponceau S (Serva) to confirm equal loading, washed twice in TBS-T (20 mM Tris, 150 mM sodium chloride, 0.1% (*v/v*) Tween 20) and blocked in 5% milk powder (Sigma) in TBS-T for 1 h at room temperature. Primary antibody incubation (5% BSA in TBS-T) was performed overnight

at 4 °C. Secondary antibodies were diluted in 5% milk powder in TBS-T, and detection was performed with enhanced chemiluminescence using an Amersham Imager 600 (GE Healthcare). The following primary antibodies were used: LDLR (rabbit monoclonal antibody; 1:1000; abcam cat. No. ab52818), CYP7B1 (rabbit monoclonal antibody; 1:1000; abcam cat. No. ab138497) and  $\gamma$ -Tubulin (rabbit monoclonal; 1:2000; cat. No. ab179503). The goat-anti-rabbit HRP coupled secondary antibody from Jackson Immunoresearch (#111-035-144) was used in a dilution of 1:5000.

### 2.7. Histology and Immunohistochemistry

For histology, liver tissues were fixed in 3.7% formaldehyde in PBS solution. Hematoxylin/Eosin, Sirius Red as well as immunohistochemistry (IHC) stainings were performed using 4  $\mu$ m sections of paraffin-embedded tissues generated by standard procedures. For IHC stainings, rat-anti-Ly6c (ab15627, abcam), rat-anti-F4/80 (MCA497, BIORAD) and rat-anti-CD3 (MCA 1477, BIORAD) primary antibodies were used, all in a dilution of 1:200 in 3% BSA (Sigma). Horseradish peroxidase (HRP) coupled donkey-anti-rat (Jackson Immunoresearch, # 712-036-153) was used as secondary antibody. After secondary antibody incubation, sections were washed with PBS for 3  $\times$  10 min. Staining was performed using an abcam DAB kit following the manufacturer's instructions. After DAB-staining, the slides were rinsed with PBS to stop the chromogenic reaction and counterstained with hematoxylin for 2 min. Slides were incubated under running tap water for 10 min to achieve bluing of the hematoxylin. Afterwards, the slides were dehydrated and mounted using Eukitt. Images were taken using a NikonA1 Ti microscope equipped with a DS-Fi-U3 brightfield camera. The Sirius Red- and F4/80-positive areas were quantified in at least six fields per section using Adobe Photoshop and ImageJ in a blinded manner as described [27]. Ly6c positive cells were quantified by counting the number of stained cells in at least six fields per section in a blinded manner.

### 2.8. Immune Cell Isolation and Staining

Spleen immune cells and liver lymphocytes were isolated as described previously [28]. Briefly, spleens were meshed through a 100  $\mu$ m cell-strainer in order to get a single cell suspension. Erythrocytes were lysed by short-term incubation of spleen cells in ACK-buffer. For the isolation of liver non-parenchymal cells (NPCs), mouse livers were perfused with PBS and mechanically dissected through a 100  $\mu$ m cell-strainer. Hepatocytes and debris were sedimented twice at 40  $\times$  g and non-parenchymal cells were recovered by centrifugation over a 35% Optiprep (Sigma-Aldrich, Taufkirchen, Germany) gradient at 400  $\times$  g. Immunofluorescence surface staining was performed with antibodies against CD3, CD4, CD8, NK1.1, CD45.2, CD11b, CD11c, Ly6C and Ly6G (all BioLegend, Koblenz, Germany). Dead cells were stained with Pacific Orange Succinimidyl Ester (Thermo Fisher Scientific, Germany) and excluded from further analysis. For intracellular cytokine staining, cells were restimulated with PMA (10 ng/mL) and ionomycin (1  $\mu$ g/mL, both Sigma-Aldrich, Germany) in the presence of GolgiPlug (1  $\mu$ L/mL, Heidelberg, Germany) for 4 h. Cells were PFA fixed and perforated in PBS containing 0.5% saponine and 2% BSA and stained for IL-17, IFN $\gamma$  and TNF (all BioLegend, Koblenz, Germany). Flow cytometry was performed using a BD LSR II cytometer (BD Biosciences, Heidelberg, Germany) and data were analyzed with FACS DIVA software.

### 2.9. Statistics

Statistical analysis was performed with Graph Pad Prism 7.0, where two-way ANOVA followed by post hoc testing (Tukey correction) was conducted. No statistical method was used to predetermine sample size. The statistical parameters (i.e.,  $p$  values, numbers of biological repeats) can be found in the figure legends. No exclusion or inclusion criteria were used for data analyses.  $p < 0.05$  was considered significant.

### 3. Results

#### 3.1. CYP7B1 Deficiency Exacerbates the Metabolic Phenotype at Thermoneutral Housing

To investigate if CYP7B1 affects MAFLD progression to steatohepatitis, wild type (WT) and *Cyp7b1*<sup>-/-</sup> mice were fed a choline-deficient high fat diet (CD-HFD) commonly used to study diet-induced steatohepatitis [29] for a period of 8 months. To elucidate whether housing temperature modulates the role of CYP7B1 during the disease's progression, littermates from both groups were housed at room temperature (22 °C) or at thermoneutrality (30 °C). Although all groups started with similar body weights, mice housed at 30 °C initially gained more weight than those at 22 °C (Figure 1A). Compared to mice housed at 22 °C, food intake was lower in mice housed at 30 °C but not different between the genotypes (Figure S1A). After 32 weeks of the CD-HFD intervention, body weight was still different between the two groups of *Cyp7b1*<sup>-/-</sup> mice but not the WT mice (Figure 1B). EchoMRI body composition analysis revealed that this was attributed to both fat and lean mass (Figure 1B). Plasma triglycerides were significantly higher in both WT and *Cyp7b1*<sup>-/-</sup> mice housed at 30 °C compared to the 22 °C-housed littermates (Figure 1C), an effect likely attributed to reduced lipid clearance by less active brown adipose tissue [30,31]. In line with this notion, thermogenic gene expression analysis of brown adipose tissues showed that *Ucp1* and *Elovl3* transcript levels were significantly lower in both genotypes upon thermoneutral housing (Figure S1B), while for *Dio2* and *Ppargc1a* this effect of thermoneutrality was only observed in *Cyp7b1*<sup>-/-</sup> mice (Figure S1B). Notably, plasma cholesterol levels were significantly higher in thermoneutral housed *Cyp7b1*<sup>-/-</sup> but not WT mice (Figure 1D). FLPC analysis showed that this was attributed mainly to the LDL lipoprotein fraction (Figure 1E). Plasma free fatty acids followed a similar, yet not significant, trend, as triglycerides and were slightly higher at thermoneutrality (Figure 1F). Similar to elevated cholesterol and LDL levels, thermoneutral housed *Cyp7b1*<sup>-/-</sup> had higher insulin (Figure 1G), plasma alanine aminotransferase activity (Figure 1H) and albumin (Figure 1I) levels. Increased albumin levels may be explained by more pronounced inflammation (see below), a state that has been shown to be associated with a prolonged plasma half-life of albumin through higher expression of the neonatal Fc receptor [32].

Together, plasma parameters indicate that at thermoneutral (but not conventional) housing temperature, CYP7B1 deficiency enhances insulin resistance, dyslipidemia and liver damage in mice fed MAFLD-inducing diet.

#### 3.2. Hepatic Lipid Accumulation and Fibrosis Are Increased in CYP7B1-Deficient Mice Housed at Thermoneutrality

Next, we studied the pathophysiological consequences of housing temperature and CYP7B1 deficiency for the liver. Notably, *Cyp7b1*<sup>-/-</sup> mice housed at 30 °C but not 22 °C had higher liver weights than the corresponding WT mice (Figure 2A). Hepatic triglyceride content was higher in mice housed at 30 °C compared to 22 °C, independent of the genotype (Figure 2B). In contrast, cholesteryl esters (Figure 2C) and diacylglycerols but no other lipid classes (Figure 2D) were exclusively higher in livers of *Cyp7b1*<sup>-/-</sup> mice at thermoneutrality.

Consistent with the hepatic triglyceride levels (Figure 2B), *Cyp7b1*<sup>-/-</sup> and WT mice housed at 30 °C exhibited a higher content of liver lipid droplets, as assessed by histology (Figure 3A). Hepatic collagen deposition, as evaluated by Sirius Red staining (Figure 3B), was higher in mice housed at thermoneutrality, although the difference reached statistical significance only in *Cyp7b1*<sup>-/-</sup> mice (Figure 3C). Using gene expression analysis, we found that several fibrosis markers (including *Timp1*, *Mmp2*, *Mmp12* and *Mmp13*) exhibited highest expression in the 30 °C-housed *Cyp7b1*<sup>-/-</sup> mice (Figure 3D).

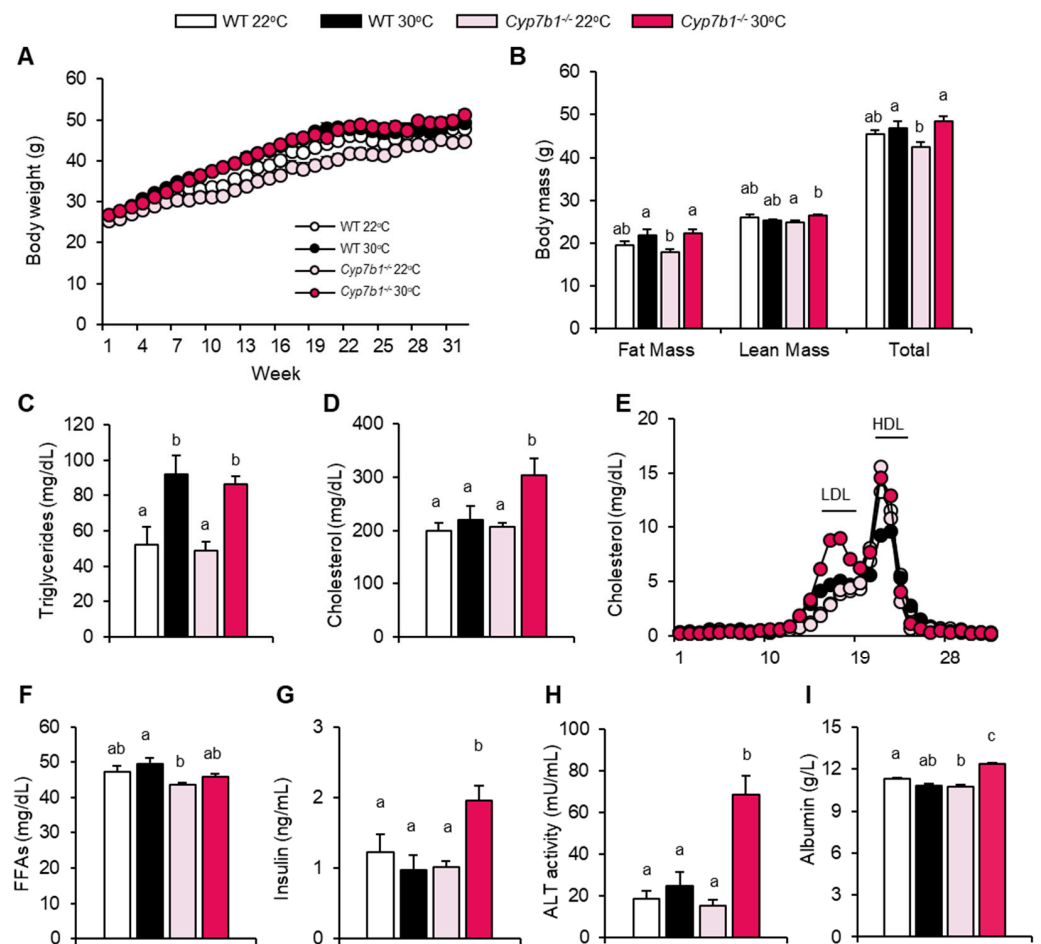


**Figure 1.** CYP7B1-deficiency induces MAFLD-associated metabolic parameters at thermoneutral housing conditions. Cyp7b1<sup>-/-</sup> and WT littermates housed under 22 °C or 30 °C were fed a CD-HFD for 8 months. (A) Body weights. (B) Body composition analysis by echoMRI. (C) Triglycerides, (D) cholesterol, (E) cholesterol in FPLC fractions, (F) free fatty acids (FFA), (G) insulin, (H) alanine aminotransferase (ALT) activity, and (I) albumin in plasma collected at the end of the feeding study. Data are shown as mean values  $\pm$  SEM (number of mice: WT 22 °C: n = 11; WT 30 °C: n = 9; Cyp7b1<sup>-/-</sup> 22 °C: n = 16; Cyp7b1<sup>-/-</sup> 30 °C: n = 13). Different letters indicate significant differences between groups ( $p < 0.05$ ) determined by two-way ANOVA.

Collectively, we observed that mice lacking CYP7B1 exhibit signs of increased MAFLD-related fibrosis and accumulate liver lipids associated with inflammation and insulin resistance [5,33] when housed at thermoneutral conditions.

### 3.3. CYP7B1 Deficiency Alters Hepatic Sterol Balance in MAFLD

CYP7B1 is a critical enzyme in the alternative bile acid synthesis pathway and affects the biosynthesis of several hydroxycholesterols. Therefore, we investigated how its deficiency would affect hepatic expression of genes related to the metabolism of bile acids and hydroxycholesterols. The bile acid synthesis genes Cyp7a1, Cyp7b1, Cyp27a1 and Cyp8b1 were lower in WT mice housed at 30 °C compared to those housed at 22 °C (Figure 4A). In the Cyp7b1 knockout mice, where we detected a truncated Cyp7b1 mRNA at lower levels but no CYP7B1 protein (Figure 4B), a similar trend was observed for Cyp27a1 and Cyp8b1. In addition, at 22 °C Cyp7a1 exhibited lower expression in the Cyp7b1<sup>-/-</sup> mice, which might be explained by an induction of its negative regulator Nr0b2 (Figure 4A). No major effects on gene expression were detected for bile acid-CoA:amino acid N-acyltransferase (BAAT) and ATP binding cassette subfamily B member 11 (ABCB11), proteins that mediate conjugation and biliary secretion of bile acids, respectively.

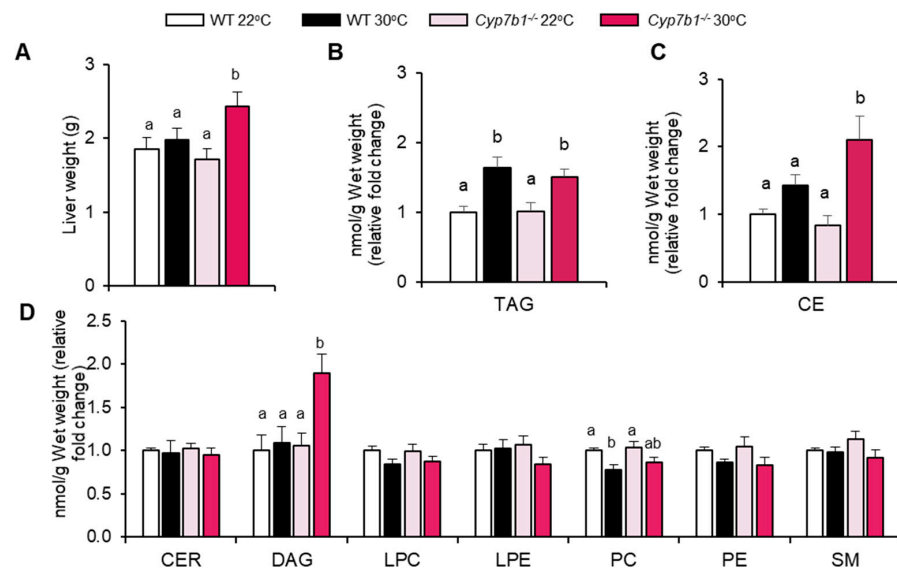


**Figure 2.** Hepatic accumulation of specific lipid classes in CYP7B1-deficient mice housed at thermoneutrality. *Cyp7b1*<sup>-/-</sup> and WT littermates housed under 22 °C or 30 °C were fed a CD-HFD for 8 months. (A) Liver weight. (B) Hepatic triglycerides (TAG) and (C) cholesteryl esters (CE). (D) Hepatic ceramides (CER), diacylglycerols (DAG), lysophosphatidylcholines (LPC), lysophosphatidylethanolamines (LPE), phosphatidylcholines (PC), phosphatidylethanolamines (PE), and sphingomyelins (SM). Data are shown as mean values ± SEM (n = 8), different letters indicate significant differences between groups (p < 0.05) determined by two-way ANOVA.

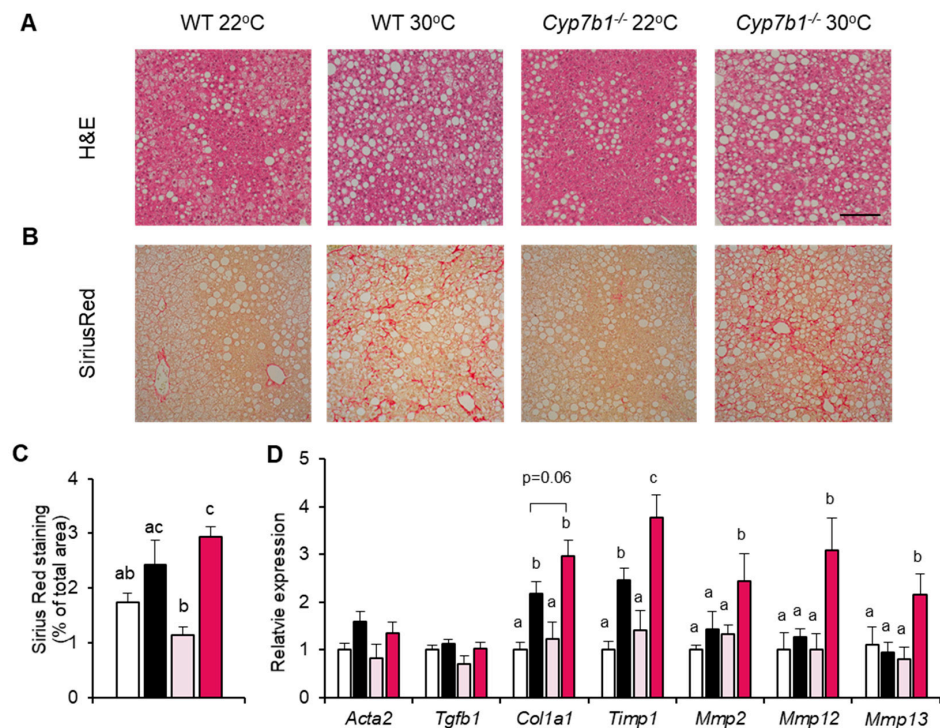


**Figure 3.** Increased fibrosis in CYP7B1-deficient mice housed at thermoneutrality. *Cyp7b1*<sup>-/-</sup> and WT littermates housed under 22 °C or 30 °C were fed a CD-HFD for 8 months. Representative images of (A) HE and (B) Sirius red stained liver sections. (C) Quantification of fibrotic areas (number of mice: WT 22 °C: n = 11; WT 30 °C: n = 9; *Cyp7b1*<sup>-/-</sup> 22 °C: n = 16; *Cyp7b1*<sup>-/-</sup> 30 °C: n = 13). (D) Hepatic expression of fibrosis-related genes normalized to *Tbp* as a housekeeper (n = 8). Data are shown as mean values ± SEM. Different letters indicate significant differences between groups (p < 0.05) determined by two-way ANOVA.

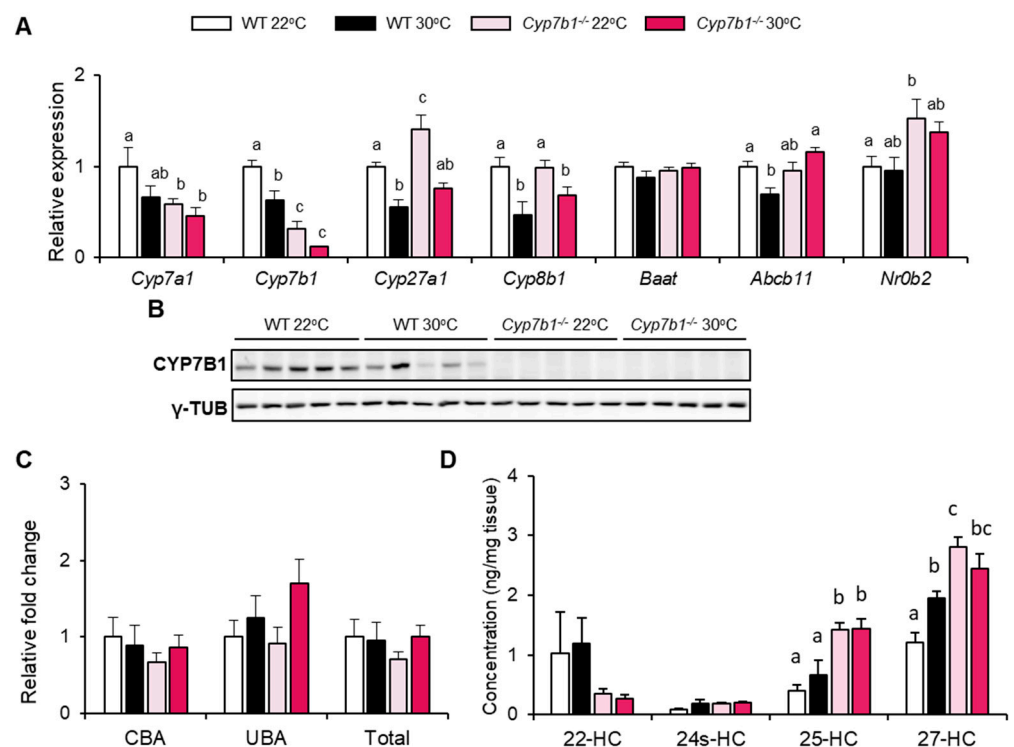


**Figure 4.** Influence of CYP7B1-deficiency on bile acid and oxysterol metabolism. Cyp7b1<sup>-/-</sup> and WT littermates were housed at 22 °C or 30 °C and fed a CD-HFD for 8 months. (A) Relative hepatic expression of bile acid- and oxysterol-related genes (n = 8). (B) Western blot analysis of hepatic CYP7B1 and the loading control gamma tubulin ( $\gamma$ -TUB). (C) Relative change of portal bile acid levels in comparison to WT 22 °C mice (number of mice: WT 22 °C: n = 11; WT 30 °C: n = 9; Cyp7b1<sup>-/-</sup> 22 °C: n = 16; Cyp7b1<sup>-/-</sup> 30 °C: n = 13). (D) Levels of hepatic hydroxycholesterol species (n = 8). Data are shown as mean values  $\pm$  SEM. Different letters indicate significant differences between groups ( $p < 0.05$ ) determined by two-way ANOVA.

Interestingly, CYP7B1 deficiency did not have a major impact on bile acid levels in portal blood (Figure 4C). In contrast to bile acids, a significant effect was observed for 27-HC and 25-HC (Figure 4D), the substrates of CYP7B1 that are generated by CYP27A1 and cholesterol 25-hydroxylase, respectively [20]. These sterols were higher in the livers of Cyp7b1<sup>-/-</sup> mice while hydroxycholesterols that are not CYP7B1 substrates (22-HC, 24s-HC) were unaltered (Figure 4D). Overall, these data indicate that CYP7B1 primarily influences hydroxycholesterol levels but has little effect on bile acid metabolism in the dietary MAFLD model.

### 3.4. Inflammatory Markers Are Increased in Cyp7b1<sup>-/-</sup> Mice upon Thermoneutral Housing Conditions

CYP7B1 deficiency affected hepatic lipid accumulation and fibrosis in thermoneutrality (Figures 2 and 3). To investigate whether these pathological alterations were accompanied by specific inflammatory responses, we performed immune cell profiling via flow cytometry analysis of the liver and spleen. In the liver, we were unable to isolate a sufficient number of viable non-parenchymal liver, which probably can be explained by excess lipid deposition and fibrosis in our 8-month feeding study. In the spleen, flow cytometry analysis revealed that Cyp7b1<sup>-/-</sup> mice had significantly increased numbers of total CD3<sup>+</sup> T cells as well as the CD8<sup>+</sup>, CD4<sup>+</sup> and CD4<sup>+</sup>CD25<sup>+</sup> subpopulations (Figure 5). A similar trend was observed for Ly6G<sup>-</sup> monocytes and Ly6G<sup>high</sup> inflammatory monocytes but not for NK, NKT cells and neutrophils. Together, these results showed that CYP7B1-deficiency modulates immune cell subpopulations in the spleen, suggesting systemic effects on inflammation.

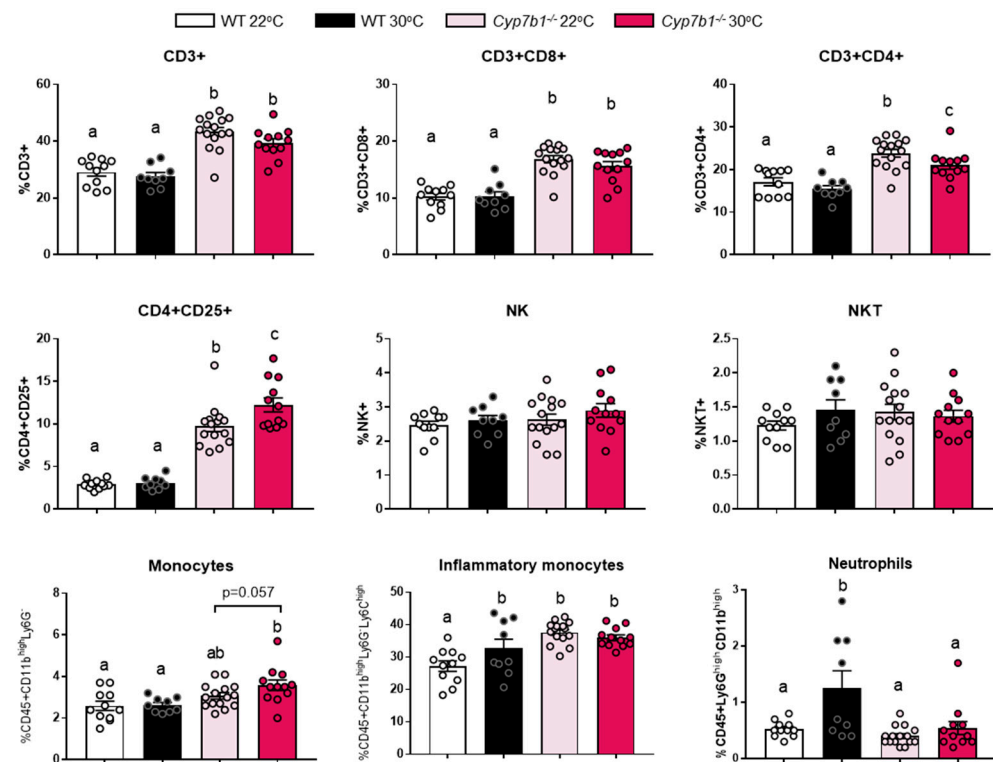


**Figure 5.** Immune cell profiling of the spleen. Flow cytometry was performed to determine CD3+, CD3+CD8+, CD3+CD4+ and CD4+CD25+ lymphocytes as well as NK, NKT, monocytes, inflammatory monocytes and neutrophils in *Cyp7b1*<sup>-/-</sup> and wild littermates type housed under 22 °C or 30 °C, all fed a CD-HFD for 8 months. Data are shown as mean values  $\pm$  SEM. (number of mice: WT 22 °C: n = 11; WT 30 °C: n = 9; *Cyp7b1*<sup>-/-</sup> 22 °C: n = 15; *Cyp7b1*<sup>-/-</sup> 30 °C: n = 12). Different letters indicate significant differences between groups ( $p < 0.05$ ) determined by two-way ANOVA.

To study the impact of CYP7B1 deficiency on immune cell infiltration into the liver, we performed hepatic immune cell profiling in *Cyp7b1*<sup>-/-</sup> and WT mice housed at 22 °C or 30 °C after CD-HFD feeding for only three weeks. This time point represents an early stage of diet-induced MAFLD, enabling efficient organ disintegration and thus flow cytometry. As in spleen the most prominent differences were observed in T lymphocytes, we studied specifically hepatic T cell subpopulations (Figure S2). Characterization of liver-infiltrating T cells by flow cytometry did not show significant differences as depicted by the comparable CD3+, CD3+CD8+ and CD3+CD4+ subpopulations (Figure S2A). However, specific analysis of isolated T cells re-stimulated with PMA/ionomycin showed that IL17- and IFN-producing CD4+ cells from *Cyp7b1*<sup>-/-</sup> mice trended to be higher. Moreover, at thermoneutrality, TNF-producing CD4+ cells were significantly elevated in CYP7B1-deficient mice in comparison to their WT littermates (Figure S2B). The respective CD8+ cytokine producing cells were unaltered (Figure S2C). These data indicate that short-term CD-HFD feeding already causes subtle changes in T cell sub-populations in livers of CYP7B1-deficient mice. To study whether CYP7B1 deficiency has effects on liver inflammation in the chronically fed mice, we analyzed the hepatic expression of inflammation-related genes including cytokines, chemokines and lymphocyte markers in WT and *Cyp7b1*<sup>-/-</sup> mice housed either at 22 °C or 30 °C. Most of the genes investigated exhibited higher expression in mice housed at 30 °C compared to those housed at 22 °C, an effect that was more pronounced in the *Cyp7b1*<sup>-/-</sup> mice than in the WT mice for *Cxcl10*, *Ccl2*, *Ccl5*, *Cd4* and *Cd8* (Figure 6A). Consistent with elevated *Cd4* and *Cd8*, a higher number of CD3-positive cells was detected via immunohistochemistry (Figure S3). As CCL2 is a critical monocyte chemoattractant, we determined infiltration of proinflammatory monocytes by immunohistology. In comparison to tissue-resident F4/80-positive Kupffer cells

(Figure 6B,D), we found increased numbers of infiltrating Ly6c-positive monocytes specifically in livers of *Cyp7b1*<sup>-/-</sup> mice housed at thermoneutrality (Figure 6C,E). A previous study showed an expansion of specific Kupffer cells characterized by high expression of *Trem2*, *Cd9*, and *Gpnmb* in NASH livers [34]. In line with this study and also with the F4/80 staining (Figure 6D), we detected higher expression of these genes at thermoneutrality (Figure 6F).

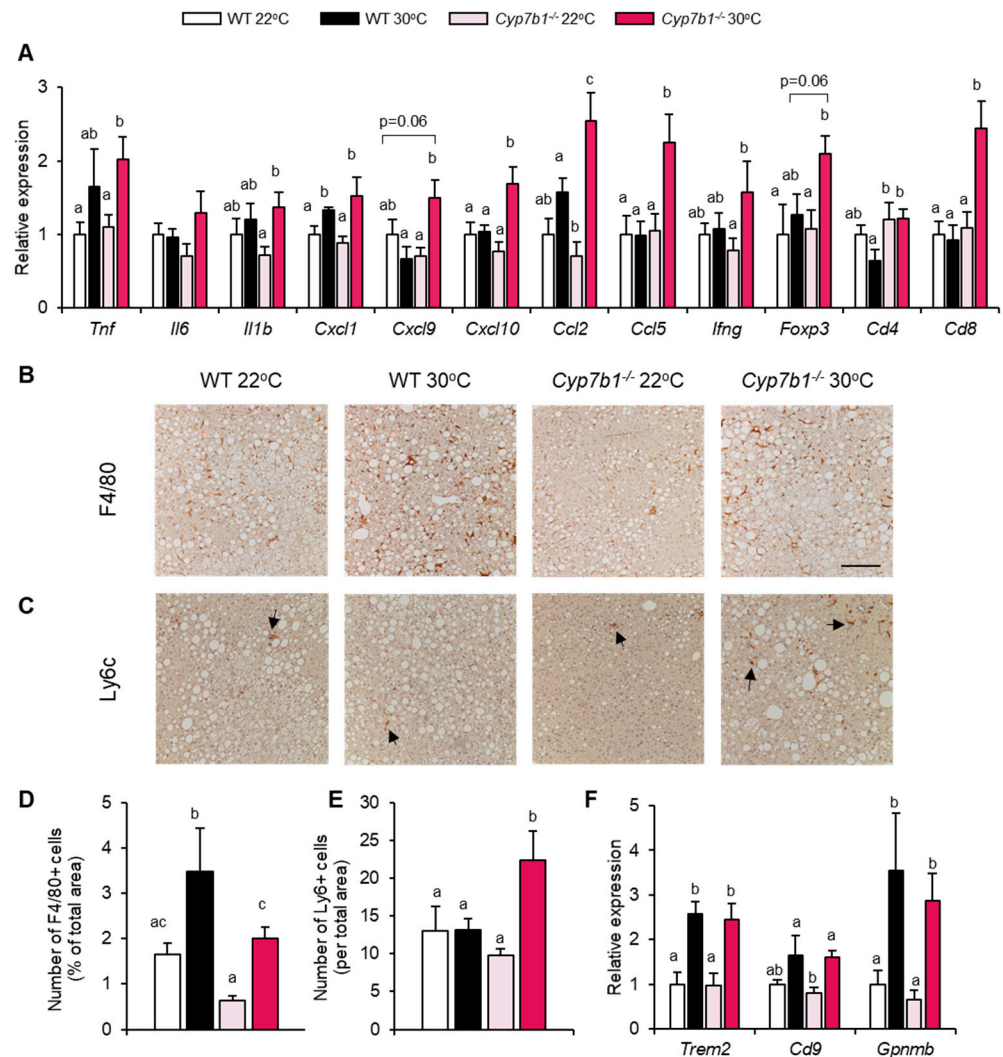


**Figure 6.** CYP7B1-deficiency leads to increased liver inflammation at thermoneutral housing conditions. *Cyp7b1*<sup>-/-</sup> and WT littermates were housed at 22 °C or 30 °C and fed a CD-HFD for 8 months. (A) Relative hepatic expression of inflammation-related and T-cell related genes (n = 8). (B,C) Representative images of (B) F4/80+ cells and (C) Ly6c+ cells (scale bar 100 μm). (D,E) Quantifications of (D) F4/80+ and (E) Ly6c+ images shown in B and C, respectively (number of mice: WT 22 °C: n = 11; WT 30 °C: n = 9; *Cyp7b1*<sup>-/-</sup> 22 °C: n = 16; *Cyp7b1*<sup>-/-</sup> 30 °C: n = 13). (F) Relative hepatic gene expression of Kupffer cell-related markers (n = 8). Data are shown as mean values ± SEM. Different letters indicate significant differences between groups ( $p < 0.05$ ) determined by two-way ANOVA.

Altogether, these results indicate that proinflammatory immune responses are exaggerated in livers of mice lacking CYP7B1 that are housed at thermoneutrality. Moreover, CYP7B1 deficiency primarily influences immune cell infiltration but not expansion of tissue-resident Kupffer cells.

### 3.5. Compensatory Lipoprotein Receptor Upregulation in CYP7B1-Deficient Mice at Room Temperature

We observed that CYP7B1-deficiency leads to lipid accumulation, proinflammatory and profibrotic responses only under thermoneutral housing conditions. Given the known role of cholesterol for MAFLD development, we studied expression of cholesterol handling proteins (Figure 7). The liver X receptor (LXR) positively regulates the transcription of hepatic cholesterol export pumps including dimeric ABCG5/ABCG8, ABCA1 and ABCG1 [35]. Despite the elevation of the LXR agonists 25-HC and 27-HC (Figure 4), expression of these genes was not affected by CYP7B1 deficiency (Figure 7A), arguing against activation of LXR under this condition. This may be explained by increased production of sulfated hydroxysterols that can act as LXR antagonists [36], as suggested by a trend for higher expression of the oxysterol sulfotransferases *Sult2a1* and *Sult2b1* at thermoneutrality (Figure 7B).

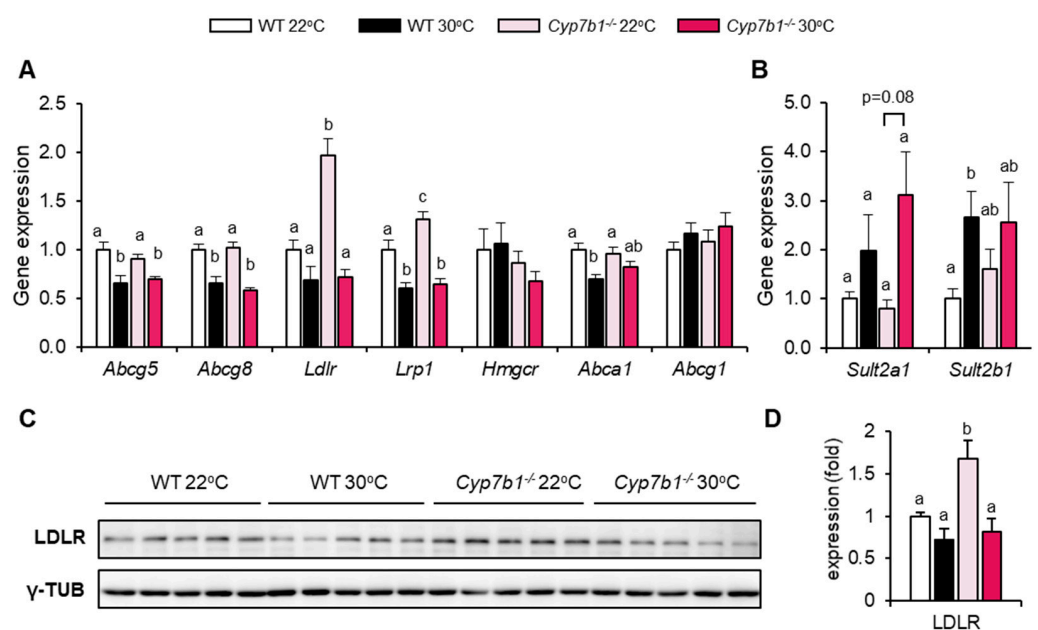


**Figure 7.** CYP7B1-deficiency affects expression of lipoprotein receptors but not other cholesterol-handling genes. *Cyp7b1*<sup>-/-</sup> and WT littermates were housed at 22 °C or 30 °C and fed a CD-HFD for 8 months. (A,B) Relative hepatic expression of (A) lipoprotein receptors and cholesterol metabolism-related genes and (B) hepatic sulfotransferases (n = 8). (C) Western blot analysis and (D) quantification of hepatic LDLR. Gamma tubulin ( $\gamma$ -TUB) was used as a loading control and for normalization. Data are shown as mean values  $\pm$  SEM. Different letters indicate significant differences between groups ( $p < 0.05$ ) determined by two-way ANOVA.

Notably, *Cyp7b1*<sup>-/-</sup> mice housed at 22 °C but not at 30 °C exhibited higher liver expression of the LDL receptor (LDLR) both at the mRNA (Figure 7A) and the protein (Figure 7C,D) level. Similarly, the LDLR-related protein-1 (*Lrp1*) was expressed at higher levels in these mice. No regulation was observed for hydroxyl-methylglutaryl-CoA reductase (*Hmgcr*), suggesting that sterol-regulatory element-binding protein-2 that positively regulates both *Ldlr* and *Hmgcr* is not responsible for the LDLR upregulation in *Cyp7b1*<sup>-/-</sup> mice housed at 22 °C.

Taken together and in line with experiments performed in LDLR deficient mice [37], these data suggest that increased flux of lipoprotein-associated lipids into hepatocytes is protective in the context of MAFLD at 22 °C. On the other hand, hepatic lipoprotein receptor expression is not induced in CYP7B1-deficient mice at thermoneutrality, favoring proinflammatory and fibrotic responses, possibly due to lipid and oxysterol accumulation in non-parenchymal and immune cells.

#### 4. Discussion

Changes in bile acid and oxysterol levels contribute and/or occur during the establishment of metabolic abnormalities such as type 2 diabetes and MAFLD [19,38]. Therefore, unravelling the contribution of specific cytochrome P450 superfamily enzymes that mediate their biosynthetic pathways can shed light on their pathophysiological role. Interestingly, the alternative bile acid synthesis pathway seems to be differentially altered in metabolic-related disorders, since CYP7B1 has been described as decreased in murine models as well as patients with type 2 diabetes [10,39,40] but was found elevated in patients with progressive MAFLD [41]. Of note, the results of mechanistic studies investigating the role of CYP7B1 in MAFLD are quite inconsistent. In a recent study, Raselli et al. pointed towards a non-essential role of CYP7B1 in MAFLD progression, as both hepatic fibrosis and disease activity score were comparable between HFD-fed WT and *Cyp7b1*<sup>-/-</sup> mice [42]. On the contrary, Kakiyama et al. provided evidence that, especially under conditions of insulin resistance, CYP7B1 could mediate progression to steatohepatitis, owing to the accumulation of toxic oxysterols that could promote inflammation and liver damage [43]. Recently, it has been shown that thermoneutral housing, a condition of low brown adipose tissue activity and diminished energy expenditure [44], provides a suitable model of exacerbated diet-induced MAFLD in mice [23]. Both Raselli et al. and Kakiyama et al. studied mice housed only at conventional room temperature. As CYP7B1 is regulated by ambient temperature [10], we aimed to understand the role of the alternative bile acid pathway in MAFLD at different housing temperatures. In the current study, we found that hepatic *Cyp7b1* expression is significantly higher in WT mice housed at 22 °C compared to 30 °C. This indicates that the alternative route of BA synthesis is higher at lower ambient temperatures, which is associated with enhanced hepatic cholesterol metabolism and accelerated lipoprotein clearance [8,9,30]. Together, these processes could explain the milder MAFLD phenotype of conventionally housed mice when compared to mice housed at thermoneutrality [23]. In line with Raselli et al. [42], CYP7B1 deficient mice housed at 22 °C have a disease phenotype upon CD-HFD feeding largely indistinguishable from their WT littermates housed at the same temperature. In contrast, we showed that *Cyp7b1*<sup>-/-</sup> mice housed at 30 °C are characterized by exacerbated MAFLD. These data indicate that CYP7B1 activity counteracts disease progression specifically under conditions of low thermogenic stress, representing typical human living conditions [20,22]. Future studies measuring parameters such as core body temperature, energy expenditure and heat loss would find it important to delineate how CYP7B1-dependent hydroxycholesterols and/or bile acids influences diet-induced energy homeostasis in the context of NASH progression.

The alternative pathway is described as a minor contributor in the biosynthesis of bile acid compared to the classical one. Previously, we have shown that hepatic CYP7B1 mRNA was moderately reduced in human liver samples of obese diabetic compared to non-obese subjects [10]. Recent publications aiming at the identification of hepatic transcriptomic signatures distinguishing simple steatosis from NASH did not report differential mRNA expression of CYP7B1 when comparing these groups [45,46]. However, the expression data do not exclude the possibility that alterations in CYP7B1 activity may aggravate MAFLD in humans. Supporting this possibility, newborns with loss of function CYP7B1 mutations develop severe liver phenotypes [47,48]. These patients lacking CYP7B1 activity are characterized by elevated levels of 24-HC, 25-HC, 27-HC, 3 $\beta$ -hydroxy-5-cholenoic and 3 $\beta$ -hydroxy-5-cholestenoic acids, aggressive hepatic fibrosis and inflammation that eventually lead to liver failure and premature death. Similarly, in our study we show that CYP7B1 deficiency in rodents leads to hepatic accumulation of the enzyme's specific hydroxycholesterol substrates 25-HC and 27-HC. All in all, the 30 °C-housed *Cyp7b1*<sup>-/-</sup> mice seem to present a hepatic milieu characterized by the accumulation of specific hydroxycholesterols. On the other hand, our data show that the 22 °C-housed *Cyp7b1*<sup>-/-</sup> mice display upregulation of *Cyp27a1* that may explain the slightly higher levels of its respective hydroxycholesterol product 27-HC. Interestingly, Bieghs et al. described that administration of 27-HC in high-fat- high cholesterol diet-fed mice can lower cholesterol-induced

inflammation and attenuate steatohepatitis over time [49]. This feature of 27-HC could, at least in part, contribute to the milder MAFLD-related phenotype in the conventional housed *Cyp7b1*<sup>-/-</sup> mice. Another explanation could be the upregulation of both *Ldlr* and *Lrp1* in CYP7B1 deficient mice housed at 22 °C but not at thermoneutrality. These lipoprotein receptors have been shown to protect against diet-induced MAFLD progression in mice [32,46,47]. Accordingly, low expression of *Ldlr* and *Lrp1* at thermoneutrality may favor lipotoxic responses mediated by accumulating lipoproteins and oxysterols.

Lipid species such as oxysterols have potent immunomodulatory functions, as they can activate several nuclear receptors (such as liver X receptors (LXRs) and retinoic acid orphan receptors (RORs)). Next to their role in regulating cholesterol and energy metabolism, these transcription factors are known to influence immune functions (including macrophage phagocytosis, T- and B-lymphocyte activation, immune cell migration and polarization [50]). Cell types of both the innate and the adaptive immune systems are important mediators of MAFLD progression [51,52]. Here, we observed a trend for increased numbers of hepatic IL17-, TNF- and INF-producing CD4+ lymphocytes in CYP7B1 deficient mice in the early stages of MAFLD progression under thermoneutral conditions. In later stages, liver stiffness and hepatic lipid accumulation prevented immune cell profiling via flow cytometry. However, immunohistology and expression analysis of inflammatory genes provided evidence that the release of specific cytokines and chemokines such as CCL2 and CCL5 by liver cells promoted the recruitment of T cells and inflammatory LyC6+ monocytes in thermoneutral housed CYP7B1-deficient mice. Importantly, these chemokines have been described to be elevated in MAFLD patients and to be important for the progression MAFLD in murine models [53,54]. Future studies are warranted to delineate the detailed mechanisms and the relevance of specific oxysterols for the regulation of immune cell subtypes in MAFLD.

In conclusion, our study demonstrates the relevance of CYP7B1 for the prevention of MAFLD and associated immunometabolic disturbances in the context of thermoneutrality. Moreover, our data suggest that stimulation of hepatic LDL receptor activity by approved pharmacological agents such as statins or PCSK9 antagonists are a testable strategy for the treatment of MAFLD in humans.

**Supplementary Materials:** The following items are available online at <https://www.mdpi.com/article/10.3390/cells10102656/s1>, Figures S1 (Relative expression of thermogenesis-related genes in brown adipose tissue) and S2 (CYP7B1-deficiency affects hepatic cytokine-producing T cell populations during the onset of MAFLD in thermoneutral conditions).

**Author Contributions:** I.E., L.S. and J.H. conceived the study and designed the experiments. I.E. performed and was involved in all experiments. D.S., P.P. and C.S. performed immune cell phenotyping experiments. A.W., C.J., J.B. and N.R. performed albumin, lipid, bile acid and hydroxysterol analysis. L.S., C.S. and J.H. supervised the experiments. The paper was written by I.E., L.S. and J.H. All authors have read and agreed to the published version of the manuscript.

**Funding:** This research was funded by German Research Foundation DFG (SFB 841, B6) and the State of Hamburg (LFF-FV75).

**Institutional Review Board Statement:** All mouse experiments were approved by the Animal Welfare Officers of University Medical Centre Hamburg-Eppendorf (UKE) and Behörde für Gesundheit und Verbraucherschutz Hamburg (G96/15).

**Informed Consent Statement:** Not applicable.

**Data Availability Statement:** The data presented in this study are openly available in Mendeley (<https://data.mendeley.com>, accessed on 4 October 2021) at DOI:10.17632/5xkrbjbb9m.1.

**Acknowledgments:** The authors thank Sandra Ehret, Birgit Henkel, Anton Hajer, Sabrina Krefß and Meike Kröger for excellent technical assistance. We thank Thomas Renné for helping us with plasma albumin measurements.

**Conflicts of Interest:** The authors declare no conflict of interest.

## References

1. Eslam, M.; Sanyal, A.J.; George, J.; International Consensus, P. MAFLD: A Consensus-Driven Proposed Nomenclature for Metabolic Associated Fatty Liver Disease. *Gastroenterology* **2020**, *158*, 1999–2014. [[CrossRef](#)] [[PubMed](#)]
2. Younossi, Z.M.; Koenig, A.B.; Abdelatif, D.; Fazel, Y.; Henry, L.; Wymer, M. Global epidemiology of nonalcoholic fatty liver disease—Meta-analytic assessment of prevalence, incidence, and outcomes. *Hepatology* **2016**, *64*, 73–84. [[CrossRef](#)] [[PubMed](#)]
3. Yki-Jarvinen, H. Non-alcoholic fatty liver disease as a cause and a consequence of metabolic syndrome. *Lancet. Diabetes Endocrinol.* **2014**, *2*, 901–910. [[CrossRef](#)]
4. Cohen, J.C.; Horton, J.D.; Hobbs, H.H. Human fatty liver disease: Old questions and new insights. *Science* **2011**, *332*, 1519–1523. [[CrossRef](#)]
5. Walenbergh, S.M.; Shiri-Sverdlov, R. Cholesterol is a significant risk factor for non-alcoholic steatohepatitis. *Expert Rev. Gastroenterol. Hepatol.* **2015**, *9*, 1343–1346. [[CrossRef](#)]
6. Kerr, T.A.; Davidson, N.O. Cholesterol and nonalcoholic fatty liver disease: Renewed focus on an old villain. *Hepatology* **2012**, *56*, 1995–1998. [[CrossRef](#)]
7. Russell, D.W. The enzymes, regulation, and genetics of bile acid synthesis. *Annu. Rev. Biochem.* **2003**, *72*, 137–174. [[CrossRef](#)]
8. Bartelt, A.; John, C.; Schaltenberg, N.; Berbee, J.F.P.; Worthmann, A.; Cherradi, M.L.; Schlein, C.; Piepenburg, J.; Boon, M.R.; Rinninger, F.; et al. Thermogenic adipocytes promote HDL turnover and reverse cholesterol transport. *Nat. Commun.* **2017**, *8*, 15010. [[CrossRef](#)] [[PubMed](#)]
9. Berbee, J.F.; Boon, M.R.; Khedoe, P.P.; Bartelt, A.; Schlein, C.; Worthmann, A.; Kooijman, S.; Hoeke, G.; Mol, I.M.; John, C.; et al. Brown fat activation reduces hypercholesterolaemia and protects from atherosclerosis development. *Nat. Commun.* **2015**, *6*, 6356. [[CrossRef](#)]
10. Worthmann, A.; John, C.; Ruhlemann, M.C.; Baguhl, M.; Heinsen, F.A.; Schaltenberg, N.; Heine, M.; Schlein, C.; Evangelakos, I.; Mineo, C.; et al. Cold-induced conversion of cholesterol to bile acids in mice shapes the gut microbiome and promotes adaptive thermogenesis. *Nat. Med.* **2017**, *23*, 839–849. [[CrossRef](#)]
11. Kuipers, F.; Groen, A.K. An unexpected role for bile acid synthesis in adaptation to low temperature. *Nat. Med.* **2017**, *23*, 800–802. [[CrossRef](#)]
12. Reboldi, A.; Dang, E.V.; McDonald, J.G.; Liang, G.; Russell, D.W.; Cyster, J.G. Inflammation. 25-Hydroxycholesterol suppresses interleukin-1-driven inflammation downstream of type I interferon. *Science* **2014**, *345*, 679–684. [[CrossRef](#)]
13. Umetani, M.; Ghosh, P.; Ishikawa, T.; Umetani, J.; Ahmed, M.; Mineo, C.; Shaul, P.W. The cholesterol metabolite 27-hydroxycholesterol promotes atherosclerosis via proinflammatory processes mediated by estrogen receptor alpha. *Cell Metab.* **2014**, *20*, 172–182. [[CrossRef](#)]
14. Santori, F.R.; Huang, P.; van de Pavert, S.A.; Douglass, E.F., Jr.; Leaver, D.J.; Haubrich, B.A.; Keber, R.; Lorbek, G.; Konijn, T.; Rosales, B.N.; et al. Identification of natural RORgamma ligands that regulate the development of lymphoid cells. *Cell Metab.* **2015**, *21*, 286–298. [[CrossRef](#)] [[PubMed](#)]
15. Hu, X.; Wang, Y.; Hao, L.Y.; Liu, X.; Lesch, C.A.; Sanchez, B.M.; Wendling, J.M.; Morgan, R.W.; Aicher, T.D.; Carter, L.L.; et al. Sterol metabolism controls T(H)17 differentiation by generating endogenous RORgamma agonists. *Nat. Chem. Biol.* **2015**, *11*, 141–147. [[CrossRef](#)] [[PubMed](#)]
16. Cui, G.; Qin, X.; Wu, L.; Zhang, Y.; Sheng, X.; Yu, Q.; Sheng, H.; Xi, B.; Zhang, J.Z.; Zang, Y.Q. Liver X receptor (LXR) mediates negative regulation of mouse and human Th17 differentiation. *J. Clin. Investig.* **2011**, *121*, 658–670. [[CrossRef](#)]
17. Hang, S.; Paik, D.; Yao, L.; Kim, E.; Trinath, J.; Lu, J.; Ha, S.; Nelson, B.N.; Kelly, S.P.; Wu, L.; et al. Bile acid metabolites control TH17 and Treg cell differentiation. *Nature* **2019**, *576*, 143–148. [[CrossRef](#)] [[PubMed](#)]
18. Song, X.; Sun, X.; Oh, S.F.; Wu, M.; Zhang, Y.; Zheng, W.; Geva-Zatorsky, N.; Jupp, R.; Mathis, D.; Benoist, C.; et al. Microbial bile acid metabolites modulate gut RORgamma(+) regulatory T cell homeostasis. *Nature* **2020**, *577*, 410–415. [[CrossRef](#)]
19. Evangelakos, I.; Heeren, J.; Verkade, E.; Kuipers, F. Role of bile acids in inflammatory liver diseases. *Semin. Immunopathol.* **2021**, *43*, 577–590. [[CrossRef](#)] [[PubMed](#)]
20. Fischer, A.W.; Cannon, B.; Nedergaard, J. Optimal housing temperatures for mice to mimic the thermal environment of humans: An experimental study. *Mol. Metab.* **2018**, *7*, 161–170. [[CrossRef](#)] [[PubMed](#)]
21. Bartelt, A.; Heeren, J. The holy grail of metabolic disease: Brown adipose tissue. *Curr. Opin. Lipidol.* **2012**, *23*, 190–195. [[CrossRef](#)]
22. Ganeshan, K.; Chawla, A. Warming the mouse to model human diseases. *Nat. Rev. Endocrinol.* **2017**, *13*, 458–465. [[CrossRef](#)]
23. Giles, D.A.; Moreno-Fernandez, M.E.; Stankiewicz, T.E.; Graspeuntner, S.; Cappelletti, M.; Wu, D.; Mukherjee, R.; Chan, C.C.; Lawson, M.J.; Klarquist, J.; et al. Thermoneutral housing exacerbates nonalcoholic fatty liver disease in mice and allows for sex-independent disease modeling. *Nat. Med.* **2017**, *23*, 829–838. [[CrossRef](#)]
24. Stahl, F.R.; Jung, R.; Jazbutyte, V.; Ostermann, E.; Todter, S.; Brixel, R.; Kemmer, A.; Halle, S.; Rose-John, S.; Messerle, M.; et al. Laboratory diagnostics of murine blood for detection of mouse cytomegalovirus (MCMV)-induced hepatitis. *Sci. Rep.* **2018**, *8*, 14823. [[CrossRef](#)] [[PubMed](#)]
25. John, C.; Werner, P.; Worthmann, A.; Wegner, K.; Todter, K.; Scheja, L.; Rohn, S.; Heeren, J.; Fischer, M. A liquid chromatography-tandem mass spectrometry-based method for the simultaneous determination of hydroxy sterols and bile acids. *J. Chromatogr. A* **2014**, *1371*, 184–195. [[CrossRef](#)] [[PubMed](#)]
26. Meljon, A.; Theofilopoulos, S.; Shackleton, C.H.; Watson, G.L.; Javitt, N.B.; Knolker, H.J.; Saini, R.; Arenas, E.; Wang, Y.; Griffiths, W.J. Analysis of bioactive oxysterols in newborn mouse brain by LC/MS. *J. Lipid Res.* **2012**, *53*, 2469–2483. [[CrossRef](#)] [[PubMed](#)]

27. Pradere, J.P.; Kluwe, J.; De Minicis, S.; Jiao, J.J.; Gwak, G.Y.; Dapito, D.H.; Jang, M.K.; Guenther, N.D.; Mederacke, I.; Friedman, R.; et al. Hepatic macrophages but not dendritic cells contribute to liver fibrosis by promoting the survival of activated hepatic stellate cells in mice. *Hepatology* **2013**, *58*, 1461–1473. [[CrossRef](#)] [[PubMed](#)]
28. Schwinge, D.; Carambia, A.; Quaas, A.; Krech, T.; Wegscheid, C.; Tiegs, G.; Prinz, I.; Lohse, A.W.; Herkel, J.; Schramm, C. Testosterone suppresses hepatic inflammation by the downregulation of IL-17, CXCL-9, and CXCL-10 in a mouse model of experimental acute cholangitis. *J. Immunol.* **2015**, *194*, 2522–2530. [[CrossRef](#)]
29. Wolf, M.J.; Adili, A.; Piotrowitz, K.; Abdullah, Z.; Boege, Y.; Stemmer, K.; Ringelhan, M.; Simonavicius, N.; Egger, M.; Wohlleber, D.; et al. Metabolic activation of intrahepatic CD8+ T cells and NKT cells causes nonalcoholic steatohepatitis and liver cancer via cross-talk with hepatocytes. *Cancer Cell* **2014**, *26*, 549–564. [[CrossRef](#)]
30. Bartelt, A.; Bruns, O.T.; Reimer, R.; Hohenberg, H.; Ittrich, H.; Peldschus, K.; Kaul, M.G.; Tromsdorf, U.I.; Weller, H.; Waurisch, C.; et al. Brown adipose tissue activity controls triglyceride clearance. *Nat. Med.* **2011**, *17*, 200–205. [[CrossRef](#)]
31. Heine, M.; Fischer, A.W.; Schlein, C.; Jung, C.; Straub, L.G.; Gottschling, K.; Mangels, N.; Yuan, Y.; Nilsson, S.K.; Liebscher, G.; et al. Lipolysis Triggers a Systemic Insulin Response Essential for Efficient Energy Replenishment of Activated Brown Adipose Tissue in Mice. *Cell Metab.* **2018**, *28*, 644–655.e4. [[CrossRef](#)]
32. Pyzik, M.; Rath, T.; Lencer, W.I.; Baker, K.; Blumberg, R.S. FcRn: The Architect Behind the Immune and Nonimmune Functions of IgG and Albumin. *J. Immunol.* **2015**, *194*, 4595–4603. [[CrossRef](#)] [[PubMed](#)]
33. Petersen, M.C.; Shulman, G.I. Mechanisms of Insulin Action and Insulin Resistance. *Physiol. Rev.* **2018**, *98*, 2133–2223. [[CrossRef](#)] [[PubMed](#)]
34. Xiong, X.; Kuang, H.; Ansari, S.; Liu, T.; Gong, J.; Wang, S.; Zhao, X.Y.; Ji, Y.; Li, C.; Guo, L.; et al. Landscape of Intercellular Crosstalk in Healthy and NASH Liver Revealed by Single-Cell Secretome Gene Analysis. *Mol. Cell* **2019**, *75*, 644–660.e5. [[CrossRef](#)] [[PubMed](#)]
35. Ma, L.; Nelson, E.R. Oxysterols and nuclear receptors. *Mol. Cell. Endocrinol.* **2019**, *484*, 42–51. [[CrossRef](#)] [[PubMed](#)]
36. Sanchez, L.D.; Pontini, L.; Marinozzi, M.; Sanchez-Aranguren, L.C.; Reis, A.; Dias, I.H.K. Cholesterol and oxysterol sulfates: Pathophysiological roles and analytical challenges. *Br. J. Pharmacol.* **2021**, *178*, 3327–3341. [[CrossRef](#)]
37. Bieggs, V.; Van Gorp, P.J.; Wouters, K.; Hendriks, T.; Gijbels, M.J.; van Bilsen, M.; Bakker, J.; Binder, C.J.; Lutjohann, D.; Staels, B.; et al. LDL receptor knock-out mice are a physiological model particularly vulnerable to study the onset of inflammation in non-alcoholic fatty liver disease. *PLoS ONE* **2012**, *7*, e30668. [[CrossRef](#)]
38. Ahmad, T.R.; Haeusler, R.A. Bile acids in glucose metabolism and insulin signaling—mechanisms and research needs. *Nat. Rev. Endocrinol.* **2019**, *15*, 701–712. [[CrossRef](#)]
39. Biddinger, S.B.; Haas, J.T.; Yu, B.B.; Bezy, O.; Jing, E.; Zhang, W.; Unterman, T.G.; Carey, M.C.; Kahn, C.R. Hepatic insulin resistance directly promotes formation of cholesterol gallstones. *Nat. Med.* **2008**, *14*, 778–782. [[CrossRef](#)] [[PubMed](#)]
40. Chen, C.; Hu, B.; Wu, T.; Zhang, Y.; Xu, Y.; Feng, Y.; Jiang, H. Bile acid profiles in diabetic (db/db) mice and their wild type littermates. *J. Pharm. Biomed. Anal.* **2016**, *131*, 473–481. [[CrossRef](#)]
41. Lake, A.D.; Novak, P.; Shipkova, P.; Aranibar, N.; Robertson, D.; Reily, M.D.; Lu, Z.; Lehman-McKeeman, L.D.; Cherrington, N.J. Decreased hepatotoxic bile acid composition and altered synthesis in progressive human nonalcoholic fatty liver disease. *Toxicol. Appl. Pharmacol.* **2013**, *268*, 132–140. [[CrossRef](#)]
42. Raselli, T.; Hearn, T.; Wyss, A.; Atrott, K.; Peter, A.; Frey-Wagner, I.; Spalinger, M.R.; Maggio, E.M.; Sailer, A.W.; Schmitt, J.; et al. Elevated oxysterol levels in human and mouse livers reflect nonalcoholic steatohepatitis. *J. Lipid Res.* **2019**, *60*, 1270–1283. [[CrossRef](#)]
43. Kakiyama, G.; Marques, D.; Martin, R.; Takei, H.; Rodriguez-Agudo, D.; LaSalle, S.A.; Hashiguchi, T.; Liu, X.; Green, R.; Erickson, S.; et al. Insulin resistance dysregulates CYP7B1 leading to oxysterol accumulation: A pathway for NAFL to NASH transition. *J. Lipid Res.* **2020**, *61*, 1629–1644. [[CrossRef](#)]
44. Heeren, J.; Scheja, L. Metabolic-associated fatty liver disease and lipoprotein metabolism. *Mol. Metab.* **2021**, *50*, 101238. [[CrossRef](#)] [[PubMed](#)]
45. Suppli, M.P.; Rigbolt, K.T.G.; Veidal, S.S.; Heeboll, S.; Eriksen, P.L.; Demant, M.; Bagger, J.I.; Nielsen, J.C.; Oro, D.; Thrane, S.W.; et al. Hepatic transcriptome signatures in patients with varying degrees of nonalcoholic fatty liver disease compared with healthy normal-weight individuals. *Am. J. Physiol. Gastrointest. Liver Physiol.* **2019**, *316*, G462–G472. [[CrossRef](#)] [[PubMed](#)]
46. Vandel, J.; Dubois-Chevalier, J.; Gheeraert, C.; Derudas, B.; Raverdy, V.; Thuillier, D.; Gaal, L.; Francque, S.; Pattou, F.; Staels, B.; et al. Hepatic Molecular Signatures Highlight the Sexual Dimorphism of Nonalcoholic Steatohepatitis (NASH). *Hepatology* **2021**, *73*, 920–936. [[CrossRef](#)] [[PubMed](#)]
47. Setchell, K.D.; Schwarz, M.; O’Connell, N.C.; Lund, E.G.; Davis, D.L.; Lathe, R.; Thompson, H.R.; Weslie Tyson, R.; Sokol, R.J.; Russell, D.W. Identification of a new inborn error in bile acid synthesis: Mutation of the oxysterol 7alpha-hydroxylase gene causes severe neonatal liver disease. *J. Clin. Investig.* **1998**, *102*, 1690–1703. [[CrossRef](#)] [[PubMed](#)]
48. Ueki, I.; Kimura, A.; Nishiyori, A.; Chen, H.L.; Takei, H.; Nittono, H.; Kurosawa, T. Neonatal cholestatic liver disease in an Asian patient with a homozygous mutation in the oxysterol 7alpha-hydroxylase gene. *J. Pediatric Gastroenterol. Nutr.* **2008**, *46*, 465–469. [[CrossRef](#)] [[PubMed](#)]
49. Bieggs, V.; Hendriks, T.; van Gorp, P.J.; Verheyen, F.; Guichot, Y.D.; Walenbergh, S.M.; Jeurissen, M.L.; Gijbels, M.; Rensen, S.S.; Bast, A.; et al. The cholesterol derivative 27-hydroxycholesterol reduces steatohepatitis in mice. *Gastroenterology* **2013**, *144*, 167–178.e1. [[CrossRef](#)]

50. Spann, N.J.; Glass, C.K. Sterols and oxysterols in immune cell function. *Nat. Immunol.* **2013**, *14*, 893–900. [[CrossRef](#)]
51. Kazankov, K.; Jorgensen, S.M.D.; Thomsen, K.L.; Moller, H.J.; Vilstrup, H.; George, J.; Schuppan, D.; Gronbaek, H. The role of macrophages in nonalcoholic fatty liver disease and nonalcoholic steatohepatitis. *Nat. Rev. Gastroenterol. Hepatol.* **2019**, *16*, 145–159. [[CrossRef](#)]
52. Sutti, S.; Albano, E. Adaptive immunity: An emerging player in the progression of NAFLD. *Nat. Rev. Gastroenterol. Hepatol.* **2020**, *17*, 81–92. [[CrossRef](#)] [[PubMed](#)]
53. Baeck, C.; Wehr, A.; Karlmark, K.R.; Heymann, F.; Vucur, M.; Gassler, N.; Huss, S.; Klussmann, S.; Eulberg, D.; Luedde, T.; et al. Pharmacological inhibition of the chemokine CCL2 (MCP-1) diminishes liver macrophage infiltration and steatohepatitis in chronic hepatic injury. *Gut* **2012**, *61*, 416–426. [[CrossRef](#)] [[PubMed](#)]
54. Berres, M.L.; Koenen, R.R.; Rueland, A.; Zaldivar, M.M.; Heinrichs, D.; Sahin, H.; Schmitz, P.; Streetz, K.L.; Berg, T.; Gassler, N.; et al. Antagonism of the chemokine Ccl5 ameliorates experimental liver fibrosis in mice. *J. Clin. Investig.* **2010**, *120*, 4129–4140. [[CrossRef](#)] [[PubMed](#)]